ARTICLES
https://doi.org/10.1038/s41477-018-0304-9

nature plants

Moisture pulse-reserve in the soil-plant continuum observed across biomes

Andrew F. Feldman[1*], Daniel J. Short Gianotti[1], Alexandra G. Konings[2], Kaighin A. McColl[3,4], Ruzbeh Akbar[1], Guido D. Salvucci[5] and Dara Entekhabi[1]

The degree to which individual pulses of available water drive plant activity across diverse biomes and climates is not well understood. It has previously only been investigated in a few dryland locations. Here, plant water uptake following pulses of surface soil moisture, an indicator for the pulse–reserve hypothesis, is investigated across South America, Africa and Australia with satellite-based estimates of surface soil and canopy water content. Our findings show that this behaviour is widespread: occurring over half of the vegetated landscapes. We estimate spatially varying soil moisture thresholds at which plant water uptake ceases, noting dependence on soil texture and proximity to the wilting point. The soil type and biome-dependent soil moisture threshold and the plant soil water uptake patterns at the scale of Earth system models allow a unique opportunity to test and improve model parameterization of vegetation function under water limitation.

Resource pulses are described as infrequent, intense, brief episodes of essential resource availability (for example, water to vegetation) that have substantial impacts on ecosystem function[1]. In the case of ecohydrology, it was previously shown that water pulses in the form of intermittent precipitation events drive plant productivity in drylands using field observations and models[2–7]. This has been studied in the context of the pulse–reserve hypothesis: a paradigm in which individual rain events induce plant growth and storage of carbon into reserves[8,9]. Even small pulses are deemed ecologically important in these dry environments[7,10–12]. Plant water uptake following pulsed water availability has been used as an indicator for this pulse–reserve behaviour with in situ measurements of xylem (or leaf) and soil potential[2,4,6,7]. Although field observations are sparse and limited to drylands[4–6], we suspect that such pulse–reserve behaviour should be prevalent across other biomes, because there is always an increased surface soil moisture availability following rainfall that decays in time (that is, drydown). However, there is limited opportunity to test the presence of this behaviour across a wider diversity of biomes and climates, especially at spatiotemporal scales of interest to Earth system models[13]. Observations of fundamental short-term plant–soil water relations are essential for understanding the transfer of water from soil to plant required for consequent transpiration and photosynthesis[14]. Additionally, since transpiration dominates the surface water exchange between land and atmosphere[15], these plant–soil water relations have a substantial role in water, carbon and energy cycles. In this study, we ask: how prevalent are plant water content responses to pulses of water availability across climates and biomes? We hypothesize that pulse–reserve behaviour is stronger in regions with herbaceous plants, possibly due to differing water use strategies (for example, rooting depth, stomatal control) between woody and herbaceous plants.

We use new satellite remote sensing observations of surface soil moisture (SM) storage (in the top 5 cm of the continuous profile) and vegetation microwave optical depth (τ) from NASA's Soil Moisture Active Passive (SMAP) satellite[16] to characterize plant–soil water relations across major continents over nearly three years (1 April 2015 to 26 December 2017). These estimates are derived from SMAP measurements of low-frequency microwave emission (L band; 1.4 GHz) from Earth's land surface using established radiative transfer theory (see Methods). The τ estimates are converted to vegetation water content (VWC) (see Methods). Estimates of τ have previously been used to evaluate seasonal plant responses[17,18], leaf water potential and isohydricity[19,20], and annual net terrestrial carbon storage[21]. Although there is vast ecosystem variability, these SMAP observations can capture the large-scale mean canopy reaction to changes in SM.

We focus our analysis on Africa, Australia and South America, which have large regions of both woody and non-woody biomes with wide ranges of climate and moisture availability. Understanding vegetation responses to perturbations in these regions is increasingly important, with climate change expected to heterogeneously alter precipitation patterns[22,23]. This may, in turn, impact the regional hydrologic cycle and carbon sequestration capacity[24,25], which is especially substantial for tropical savannahs/grasslands in these regions[26,27]. We find large-scale observational evidence for the pulse–reserve hypothesis in 52% of the vegetated area in the study regions. While pulse–reserve behaviour is most vigorous and prevalent in the driest regions with sparse tree cover, the same mechanism still persists, albeit less commonly and at a weaker level, in regions with up to approximately 1,000 mm of annual rainfall and 20% tree cover. Further, we find that this pulse–reserve behaviour occurs only if the surface is sufficiently wet above a threshold. We estimate the SM thresholds and find that they are correlated with clay fraction and analogous to, but lower than, the standard wilting point value of −1.5 MPa commonly used in modelling studies[28].

Results

Plant water content increases during drydowns only in soils above an SM threshold. With SMAP remote sensing measurements, we can assess the large-scale plant water response to short-term surface

[1]Department of Civil and Environmental Engineering, Massachusetts Institute of Technology, Cambridge, Massachusetts, USA. [2]Department of Earth System Science, Stanford University, Stanford, California, USA. [3]Department of Earth and Planetary Sciences, Harvard University, Cambridge, MA, USA. [4]Harvard John A. Paulson School of Engineering and Applied Sciences, Harvard University, Cambridge, MA, USA. [5]Department of Earth and Environment, Boston University, Boston, MA, USA. *e-mail: afeld24@mit.edu

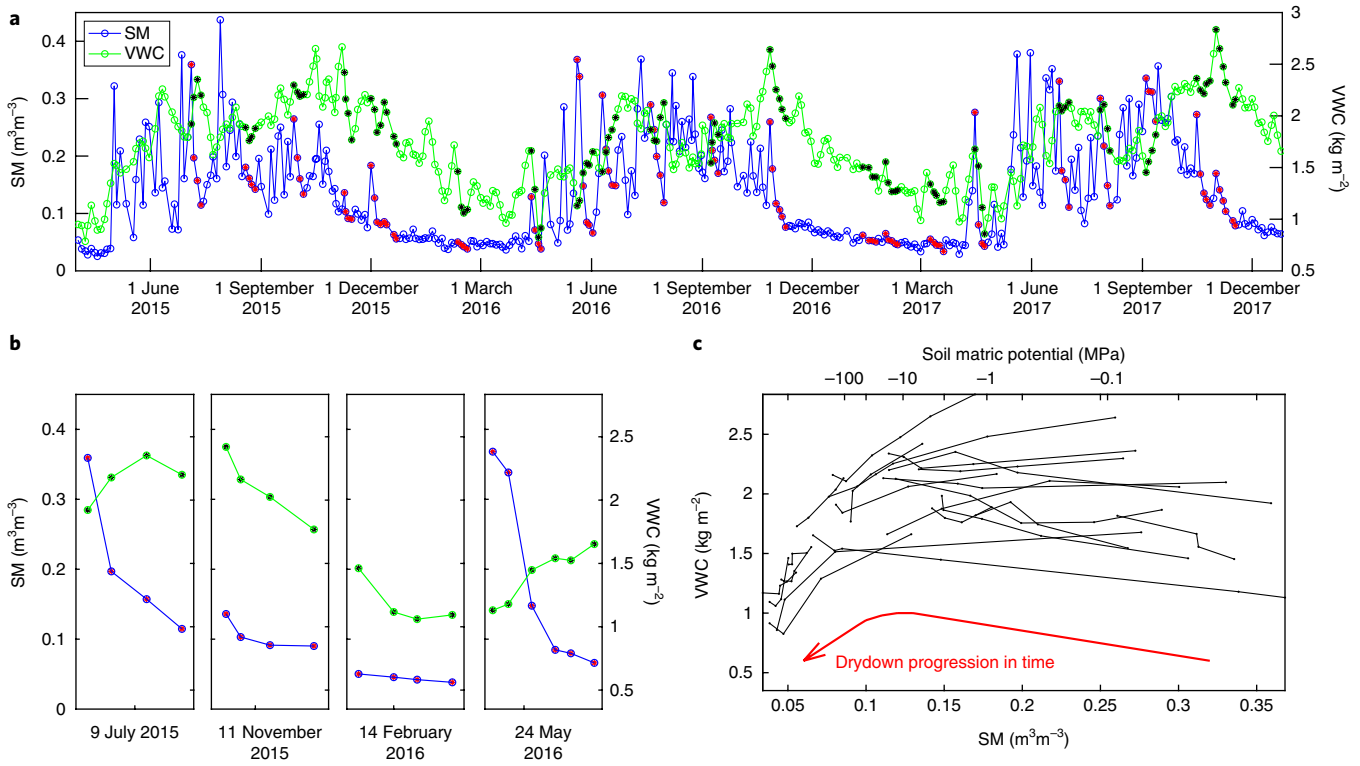

Fig. 1 | Plant–soil water relationship at an example location (9.1° N, 27.2° E; South Sudan). a, SM and VWC time series with SM drydowns marked with red symbols and simultaneous VWC values denoted with black stars. **b**, Example VWC–SM drydowns from the full time series. **c**, VWC–SM phase plot of (SM, VWC) pairs during all SM drydowns. During SM drydowns (decreasing SM), VWC increases when the soil is wet and decreases when the soil is dry. SM is converted to soil matric potential for reference (see Methods).

SM variability. Previous work noted that the pulse–reserve paradigm should assess plant response to pulses of soil water, which account for antecedent soil water availability[2]. Thus, we use SM rather than the more commonly used precipitation to characterize individual events. Specifically, only SM drydowns, defined as at least four consecutive SMAP observations (over ≥12 days) of decreasing SM, and simultaneous VWC estimates are considered. These are drying periods with negligible precipitation following SM accumulations from previous rainfall and have been characterized globally with SMAP measurements[29]. Figure 1 shows an example time series over a single 9 km pixel in South Sudan. SM and VWC values during identified SM drydowns are labelled with magnified individual examples shown in Fig. 1b. If all (SM, VWC) pairs during SM drydowns from the nearly three-year time series are plotted in phase space (Fig. 1c), a nonlinear relationship between plant and soil water emerges, with threshold behaviour depending on SM. This suggests that during an SM drydown, when the surface is initially wet (following red arrow in Fig. 1c), VWC increases—implying that plant uptake and storage of SM exceeds transpiration—or stays constant. Once SM falls below a threshold (shown later to depend on soil texture and its hydraulic properties), the plant water uptake decreases and its dynamics switch sign with vegetation moisture loss.

To assess biome-dependent VWC behaviour, all drydowns from pixels within each biome (selected biomes shown in Supplementary Fig. 1; based on International Geosphere-Biosphere Programme (IGBP) land-cover classifications) are plotted on the same phase space, as shown in Fig. 2. Only biomes in Africa are shown, although similar results are obtained for Australia and South America. The phase space is discretized and the median drydown of all drydowns originating from discrete points in the VWC–SM phase space is reported. Additionally, the median ΔVWC/ΔSM for each drydown is reported as the symbol fill colour. The seasonal cycle is removed from SM and VWC to both remove effects of seasonal changes in biomass and isolate the short-term response of the vegetation to pulses of soil water availability (Methods). Other biomes, which exhibit behaviour similar to grasslands in Fig. 2a, are shown in Supplementary Fig. 2. For the biomes with primarily herbaceous vegetation (that is, grasslands in Fig. 2a and other biomes in Supplementary Fig. 2), moving from right to left on the diagram in time (refer to red line in Fig. 1c), plants appear to increase their water content when SM is available and lose water when SM is lower than a threshold. Red symbols (ΔVWC/ΔSM < 0) represent plant water increasing while SM is decreasing. Blue symbols (ΔVWC/ΔSM > 0) represent plant water loss while SM is decreasing. These observations suggest a large-scale plant response of net water storage (where root water uptake exceeded transpiration) over a period of three days during SM drydowns above an SM threshold. The behaviour shown in Figs. 1c and 2a also occurs in drydowns over two weeks in length, suggesting persistence of this pulse–reserve paradigm over this timescale. This behaviour appears consistent with measured xylem or leaf potential responses of semi-arid grasses and shrubs after rainfall events[5,6,30]. Further, the increase in VWC may be accentuated (darker red symbols) when VWC is low and SM high (see Supplementary Fig. 2). This is consistent with modelling studies in which a lower leaf water potential (monotonically related to VWC[19]) and increased soil water potential (monotonically related to SM) can result in vigorous pressure-driven moisture exchange in the soil–plant continuum and consequent plant water storage[2,31,32]. This overall behaviour can be modelled within soil–plant–atmosphere continuum (SPAC) models, which use unsaturated zone dynamics and cohesion tension theory[32,33] and depend on the accurate parameterization of atmospheric and stomatal controls[32].

In woody savannahs (Fig. 2b), which contain a higher presence of forest cover, plants generally either do not react to SM availability or

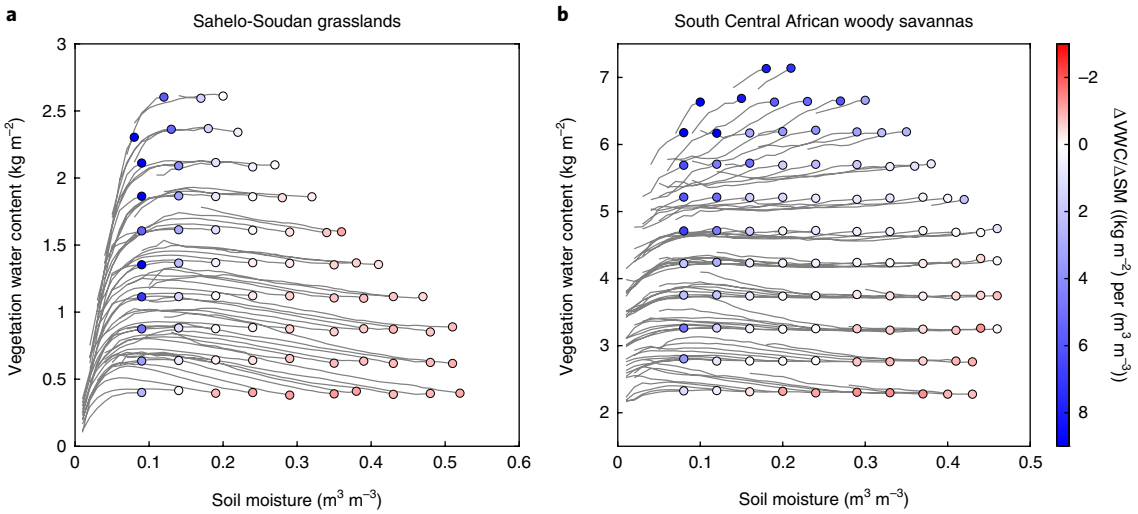

Fig. 2 | Biome-dependent plant–soil water relations during SM drydowns. a, Grasslands from Sahelo-Soudan region. **b**, Woody savannahs from South Central Africa. These regions are delineated in Supplementary Fig. 1. Each curve traces in time from high to low SM (right to left) and represents the median path of all drydowns starting from that initial condition (symbol) in the phase space. The symbol fill colour is the median ΔVWC/ΔSM slope for the corresponding curve starting at that point in VWC–SM space. Red (blue) fill represents increasing (decreasing) VWC in time during the SM drydown. See Supplementary Fig. 2 for three other biomes. Note that axis limits are adjusted to the respective biome's phase space limits, which are not consistent across biomes.

lose water. However, when VWC is overall lower (VWC < 4 kg m^{-2}) due to a lower density of woody vegetation and/or a dried vegetation state, similar behaviour to that in grasslands is exhibited (Fig. 2b). The contrasting behaviour in Fig. 2a,b can be partially explained by the fact that herbaceous plants (Fig. 2a) typically have been found to have a shallow rooting depth and preferentially use water from the nutrient-rich upper soil layers (<20 cm)[34–36]. This is despite rooting distributions generally extending past 50 cm within these regions[37,38]. Thus, herbaceous plant water should be sensitive to SM variations in the top 5 cm of soil.

Estimated soil moisture thresholds for plant water uptake are consistent with wilting point estimates. Once the surface dries, a water loss condition arises whereby plants are unable to store/retain available water at such a low soil water potential[31]. We estimate the SM threshold at which biome response to SM pulses switches from gaining to losing plant water during drydowns (that is, SM value at ΔVWC/ΔSM = 0). A threshold is computed over each pixel, performing the analysis at a 0.5° resolution (see Methods). The absolute values are displayed for each region in Supplementary Fig. 3. The SM threshold median of 0.13 m^3 m^{-3} is consistent with limited known plant measurements[39]. Also, spatial variability is related to soil texture with a positive correlation with clay fraction (Fig. 3a, Pearson's correlation coefficient $r = 0.51$; $P < 0.01$) and a negative correlation with sand fraction (not shown, $r = -0.47$; $P < 0.01$), as expected. Additionally, there is a tendency for higher SM thresholds with greater annual rainfall (not shown, $r = 0.37$; $P < 0.01$) and tree cover (not shown, $r = 0.44$; $P < 0.01$), suggesting possible drought adaptation by herbaceous plants[40].

Using sand and clay fraction and the estimated SM thresholds, a corresponding soil matric potential threshold is estimated (see Methods). These values at which plants overall lose water occur at a median of −3.0 MPa, but with wide variability (Fig. 3b; spatial maps shown in Supplementary Fig. 4), possibly related to plant functional type (Fig. 3c). This ultimately provides regional estimates of a plant hydraulic limit that are possibly related to the wilting point, or the moisture level at which wilting ensues unless the plant is resupplied with water. While the wilting point is typically defined as −1.5 MPa, our estimated limits are consistent with wilting point estimates of around −3 MPa in African savannahs[40] and commonly reaching −10 MPa in dryland species[8]. Further, stomatal conductance models suggest that this threshold may also vary in time depending on abiotic variables (for example, temperature, solar radiation, vapour pressure deficit)[41].

Pulse–reserve behaviour is most vigorous for biomes with lower rainfall and tree cover. During SM drydowns above the estimated SM threshold, plant water is expected to generally increase (ΔVWC/ΔSM < 0) based on results in Figs. 1 and 2. Thus, the responsiveness of vegetation to SM pulses, or the degree to which plant water increases during a drydown, can be assessed based on the magnitude of the ΔVWC/ΔSM slope. For each 0.5° pixel, the median ΔVWC/ΔSM slope above the corresponding SM threshold estimate in Supplementary Fig. 3 is computed and reported in Fig. 4a–c. The presence of negative ΔVWC/ΔSM values indicates pulse–reserve plant behaviour, which occurs away from humid, forested regions (for example, the Amazon and Congo Basins). The most negative ΔVWC/ΔSM values correspond to vegetation that responds with a more vigorous increase of VWC with a pulse of moisture availability (for example, the Sahel, Southern Africa, Outback Australia). Figure 4d–f shows that this typically occurs for biomes dominated by herbaceous plants, especially in shrublands and grasslands, characterized by lower tree cover and annual rainfall. While biomes with lower rainfall and tree cover exhibit the strongest, most prevalent pulse–reserve behaviour, regions with up to around 1,000 mm of annual precipitation and 20% tree cover still show the same behaviour. Prevalence is defined as percentage of possible vegetated pixels with robust pulse–reserve behaviour, indicated by bold percentages over the respective bins in Fig. 4d–f. This suggests that the pulse–reserve paradigm—previously only investigated in the driest regions, such as the Sonoran and Mojave Deserts[2]—exists on a spectrum, with the strength and prevalence of behaviour decreasing with higher annual water availability and presence of woody vegetation. Regions with greater tree cover and rainfall than this typically have no estimated SM threshold and no pulse–reserve behaviour; plant–water behaviour is probably mediated by other factors, such as shallow groundwater[42]. Thus, pulse–reserve behaviour is more widespread than previously thought. Specifically, it dominates 52% of the vegetated area across the regions studied.

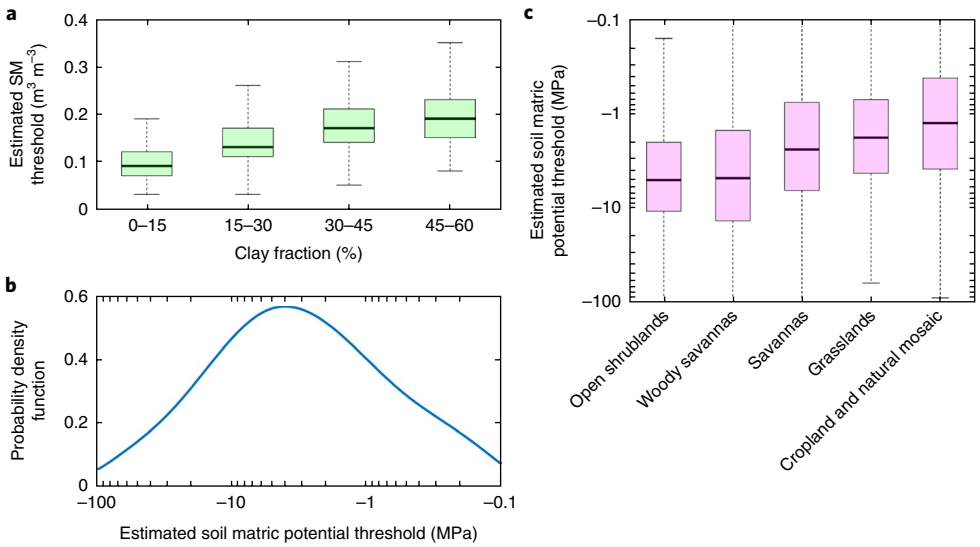

Fig. 3 | Estimated soil moisture and matric potential thresholds below which plants lose water. a, This SM threshold estimate correlates positively with clay fraction ($r = 0.51$; $P < 0.01$). Note that few pixels have clay fractions greater than 60%, and thus they are not represented in the bins. Bin counts are all greater than 500. **b**, Probability density function of estimated soil matric potential threshold. **c**, Matric potential threshold dependence on biome type. Bin counts are all greater than 400. Box edges are the 25th and 75th percentiles of the distribution bounding the median (bold line), and whiskers extend to extrema (maximum and minimum). See Supplementary Fig. 7 for uncertainty bounds generated with bootstrapping.

Positive ΔVWC/ΔSM values are unusual and typically occur in transition regions near forests (that is, near the Congo Basin, West African coast, Amazon Basin) or extremely arid areas (that is, the Sahara Desert). In these instances, ΔVWC/ΔSM slopes above the threshold are a mix of positive and negative values. Thus, positive ΔVWC/ΔSM values are ultimately not interpreted as pulse–reserve behaviour in overall metrics and should be considered with caution. Biomes with lower tree cover also exhibit the most vigorous decreases in VWC during SM drydowns (that is, greater ΔVWC/ΔSM > 0; darker blue) below the estimated SM threshold (see Supplementary Fig. 5).

Pulse–reserve plant water uptake findings are robust to estimation errors. Multiple tests are conducted to evaluate the robustness of our results. The SM and VWC seasonal cycles are removed from all parts of the analysis (except for SM threshold estimation; see Methods) to establish that the nonlinear relationships between SM and VWC are not a result of confounding variables (for example, solar radiation; see Supplementary Fig. 6). Additionally, the possibility of compensation or correlation between SM and VWC within the simultaneous estimation is investigated (see Methods). Ultimately, introducing both random and correlated error under different scenarios into the simultaneous SM and VWC estimation results in positive correlations in SM and VWC errors across multiple randomly selected pixels, especially during drydowns during wetter periods (the time periods relevant to our analysis). The negative ΔVWC/ΔSM slopes obtained here (Fig. 4) are of the opposite sign and are therefore probably capturing a physical response that even overcomes the positive correlation contribution from any estimation compensation. Further, any simultaneous estimation errors probably reduce the strength of the negative ΔVWC/ΔSM slopes, decreasing the significance of the pulse–reserve behaviour. The analysis was repeated using the SMAP baseline SM product, derived with a completely independent retrieval method and specifically not derived simultaneously with VWC (see Methods). This yields nearly identical results and suggests that these results are not an artefact of mathematical interplay between SM and VWC during the simultaneous estimation. Finally, bootstrapping is conducted on SM threshold and ΔVWC/ΔSM estimates, revealing robust estimates for both variables across all regions (see Methods and Supplementary Fig. 7). Specifically, 82% of pixels that have an SM threshold (that is, all pixels with a finite value plotted in Fig. 4) have robust pulse–reserve behaviour, where robustness is defined as having a negative 90th percentile ΔVWC/ΔSM value. See Methods for more information on these assessments.

Discussion

This study presents large-scale observations of short-term plant–soil water relations following SM pulses (caused by individual or collections of storm events). Our findings suggest that the pulse–reserve hypothesis is not specific to drylands, but is a prevalent mechanism across over half of the vegetated landscapes of Africa, South America and Australia. This suggests that individual SM accumulations drive plant activity in these regions, as observed at daily to weekly timescales. However, the observed plant water uptake only occurs if the surface is sufficiently wet. The existence of threshold behaviour was the subject of previous attention in aridland ecology[3,9,12]. Our results suggest that ecologically important events for plant water uptake in this context are pulses that increase SM above thresholds as quantified in Fig. 3[2,3,12]. SM thresholds for soil microbial activity and tree establishment may be lower and higher, respectively[12]. Our large-scale estimates of SM thresholds are possibly related to the wilting point, but show wide variability and a lower median than the values assumed in previous applications[8,40]. Our results also show a tendency for lower thresholds in drier environments, suggesting possible drought adaptations.

While the pulse–reserve behaviour extends into regions with roughly 1,000 mm of annual precipitation and 20% tree cover, a limit is eventually reached where this behaviour no longer occurs. We speculate that this is due to more prevalent woody vegetation above this limit, for the following reasons. First, woody plants have a longer uptake response time due to a longer time period for an SM pulse to penetrate to their deeper roots, as previously postulated based on a model[3]. Since we are only evaluating immediate plant responses, a lagged VWC response on the order of weeks may be missed. Second, trees have been generally found to have greater stomatal control than shrubs and grasses[19,43], dampening short-term plant response to available SM. Third, in general, a greater fraction

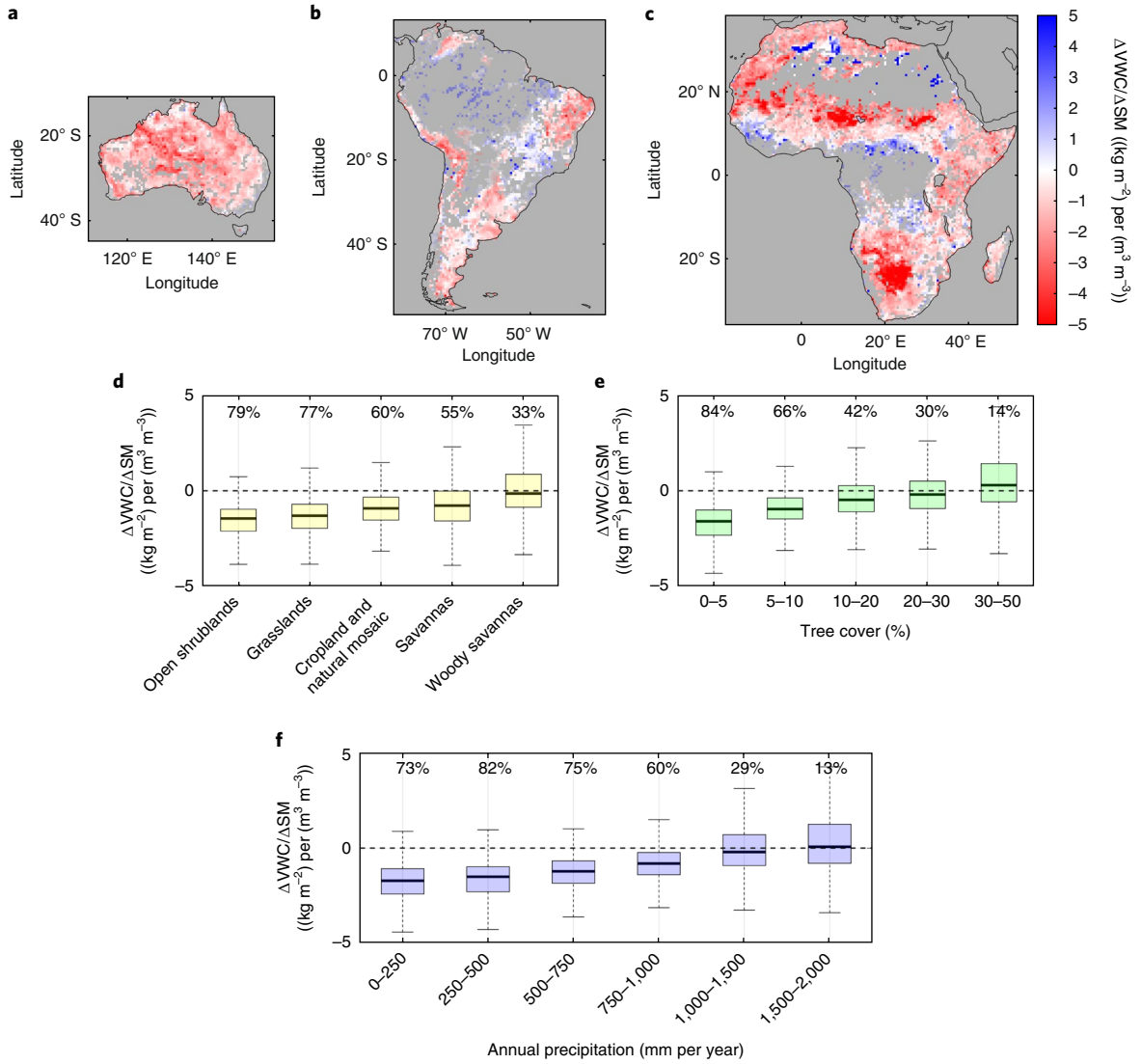

Fig. 4 | Responsiveness of vegetation to pulses of available soil water. a–c, Australia (**a**), South America (**b**) and Africa (**c**). Above the estimated SM threshold (shown in Supplementary Fig. 3), VWC increases as SM decreases during SM drydowns, resulting in the negative ΔVWC/ΔSM slope (red) as shown here (for discussion of exceptions in blue, see text). A more negative slope (darker red) suggests that vegetation is more responsive to SM pulses. Grey shading indicates masked values due to water body fraction greater than 5% or no SM threshold present. Pixels with dense vegetation (for example, the Congo Basin, West African coast and the Amazon Basin) are transparent and generally have no SM threshold. **d–f**, Vegetation responsiveness to SM pulses is greatest in regions with herbaceous vegetation land cover (**d**), lower tree cover (**e**) and lower annual rainfall (**f**). The prevalence of robust pulse–reserve behaviour decreases with increasing precipitation and tree cover. This is shown by the bold numbers above each bin in **d**, **e** and **f**, which are the percentages of vegetated pixels within the bin that show robust pulse–reserve behaviour (where robustness is defined as the bootstrapped 90th percentile ΔVWC/ΔSM value being negative). Box edges are the 25th and 75th percentiles of the distribution bounding the median (bold line), and whiskers extend to extrema (maximum and minimum). All boxplot bin counts are greater than 350. See Supplementary Fig. 7 for uncertainty bounds generated with bootstrapping.

of root biomass occurs in the top 30 cm for grasslands than for woody biomes[37]. However, most plant species across the tropics are able to access deeper water reserves (>50 cm)[37,38], with variability in rooting depth probably explained by the interplay of topography and water table depth rather than plant species[44]. Further observational evidence is required to support these assertions.

The continental-scale detection and estimation of (1) the SM threshold for plant water uptake and (2) the dynamics of vegetation water storage during drydowns (including a switch in sign of storage change) are important aggregate responses that may serve as guidance for testing and improving the representation of vegetation function in SPAC and Earth system models. Representations using a single value of wilting point (most commonly −1.5 MPa)[28] should account for the wide variability and dependence on climate, biome type and soil texture implied by the estimated SM thresholds (Fig. 3 and Supplementary Figs. 3 and 4). Additionally, the results on the extent and vigour of canopy soil water uptake estimated in this study (Fig. 4) provide an opportunity to test whether vegetation models with dynamic plant hydraulic representation show realistic vegetation water uptake patterns and threshold behaviour. This includes models such as TREES[45], ED2-hydraulics[28] and SPAC models[32], where VWC observations in this context can be evaluated as a combination of biomass and leaf water potential[20]. With advances in plant hydraulic theory and models, elements of non-steady-state water transport in the soil–plant continuum may merit inclusion in land surface parameterizations within Earth system models[13]. The results shown here can guide development and validation at the scale of these models.

Methods

Datasets. The SMAP passive microwave L1C brightness temperature product from 1 April 2015 to 26 December 2017 is the primary dataset used in this study[46]. The SMAP radiometer makes measurements at an approximately 40 km resolution (−3 dB or half-power definition) and two- to three-day revisit depending on latitude[16]. The measurements used in this study are made consistently at about 6:00. The product was recently enhanced to achieve slightly better resolution where there is substantial instrument oversampling and is gridded on a 9 km Equal-Area scalable Earth-2 (EASE-2) grid using the Backus–Gilbert optimal interpolation technique[47]. Ancillary physical temperature data obtained from a numerical weather model and soil clay and sand fraction are used for algorithm estimates of SM and VWC[46].

Annual precipitation is obtained from two years of NASA's Global Precipitation Measurement (GPM) mission between 1 April 2015 and 31 March 2017[48]. Tree-cover fraction estimates are based on measurements by the Moderate Resolution Imaging Spectroradiometer (MODIS) during 2016[49]. These datasets are re-gridded to the 9 km EASE-2 grid and used to evaluate woody plant responsiveness to SM pulses. IGBP land-cover classifications are used to separate biome-dependent responses to SM pulses[50].

Retrieval of SM and VWC. The SMAP radiometer measures the horizontally and vertically polarized (wave emission excited in the horizontal and vertical directions, respectively) brightness temperature, which are distinguished at the satellite's 40° incidence angle. The tau–omega model, a well-established radiative transfer model in the passive microwave remote sensing community, is used to partition between the surface soil and vegetation signals[51]. The multitemporal dual channel algorithm (MT-DCA), developed previously, was used here to robustly retrieve SM and τ from dual-polarized brightness temperature measurements[52,53].

The MT-DCA is implemented over all 9 km EASE-2 pixels in Africa, Australia and South America over the study period, retrieving a time series of τ and SM. Since τ is linearly proportional to VWC, τ is divided by a constant of proportionality assumed to be 0.11 across all biomes (values deviate minimally from 0.11 across biomes at this microwave frequency, and results are not sensitive to this constant value) to convert to VWC[54,55]. We expect that the measurement time of 6:00 should dampen the variable effects of nocturnal vegetation water activity and vapour pressure deficit during the day. Pixels with standing water body area dominating more than 5% of the pixel are removed. Measurements during freezing temperatures are also removed from the analysis. Note that τ is assumed to be polarization independent, which is a viable assumption at resolutions approaching tens of kilometres, especially over these continents, where vegetation patterns are primarily random with little anisotropy (unlike, for example, croplands and managed forests)[56].

The analysis in this study is repeated with the SMAP baseline SM product in lieu of the MT-DCA algorithm SM estimates as a check for the robustness of results[57]. Unlike the MT-DCA, the SMAP baseline SM product uses ancillary data to estimate VWC and hence its SM estimates do not interplay in any form with the MT-DCA τ estimates.

Characterization of SM drydowns and VWC–SM phase space. In all parts of the analysis, only SM and VWC during SM drydowns are evaluated. SM drydowns are defined as at least four consecutive overpasses with SM less than the previous overpass ($SM_{j+1} < SM_j$, where j is the index of the overpass within each drydown). The choice of four consecutive overpasses is a balance between removing short unphysical SM drydowns due to radiometer noise and avoiding a bias of only evaluating the longest drydowns. Precipitation observations over these regions, especially Africa[58], are uncertain, given the current sparse network of rain stations, and are not used to characterize drydowns in this study.

In Figs. 2–4 and Supplementary Fig. 2, SM drydowns are identified within each pixel, and the effect of the seasonal cycle of SM and VWC is removed to avoid the effect of confounding variables (for example, solar radiation) on VWC–SM relationships. The seasonal cycle of SM was not removed during estimation of the SM and soil matric potiental (ψ) thresholds, as these require absolute values of SM. However, we found that removing the SM seasonal cycle using the following methods had negligible impacts on SM and ψ threshold estimates. If two variables share the same periodicity but are shifted in phase, their phase space will be a loop[59]. Removing the seasonal cycle of SM and VWC ensures that the observed VWC–SM behaviour is due to sub-seasonal linkages between the vegetation and soil water dynamics. To identify the mean seasonal cycle of SM and VWC, the three years of each time series are averaged into a mean climatology and smoothed using a 90-day moving average filter. This mean annual climatology is replicated across the length of the nearly three-year period in this study. The increments of changes in smoothed VWC (that is, $VWC_{j+1} - VWC_j$ during a SM drydown), which are typically small (see Supplementary Fig. 6), are subtracted from the increments of changes of the raw VWC. The same process is repeated for SM during the drydown.

The VWC–SM phase diagrams in Fig. 2 and Supplementary Fig. 2 are obtained by considering only the drydowns from pixels highlighted in Supplementary Fig. 1, selected based on region size and the same seasonal climatology for each of the five primary IGBP land-cover classifications evaluated here. The phase space is discretized into 12 equally spaced increments, referred to here as blocks, along each axis, depending on the bounds of possible SM and VWC values for each classification. SM is linearly interpolated to a 0.01 $m^3 m^{-3}$ scale to allow consistent comparison of VWC values between all SM drydowns. Simultaneous VWC values are also linearly interpolated, coinciding with the interpolated SM drydown, in 0.01 $m^3 m^{-3}$ increments. All SM drydowns that originate in each respective block are concatenated. The median SM and VWC pairs for each SM increment are determined and plotted, with the initial point denoted as a filled symbol. The fill colour corresponds to the value of the median ΔVWC/ΔSM increment (for example, $(VWC_{j+1} - VWC_j)/(SM_{j+1} - SM_j)$) between each overpass for drydowns originating in the respective discretized block. If fewer than 100 drydowns occur within a block, no VWC–SM drydown is reported.

SM and soil matric potential threshold estimation. A pixel-by-pixel analysis is conducted and VWC–SM phase space is evaluated to determine the SM threshold value when ΔVWC/ΔSM switches from negative to positive during the SM drydown. To increase the sample size of drydowns, the analysis was performed at a 0.5° resolution. Thus, drydowns from all 9 km pixels within each 0.5° pixel are compiled with SM and VWC values interpolated with the same method as above. The median VWC value is computed across each 0.01 $m^3 m^{-3}$ SM increment to obtain a median VWC–SM drydown. 0.01 $m^3 m^{-3}$ SM increments with fewer than five corresponding VWC values are excluded. The VWC–SM drydown is smoothed using a moving average filter window of 0.05 $m^3 m^{-3}$. The SM value at the maximum VWC is the estimated SM threshold as displayed in Fig. 3 and Supplementary Fig. 3. If there are fewer than 50 ΔVWC/ΔSM increments on either side of the threshold within the 0.5° pixel, no SM threshold is reported, noting that no peak or only spurious peaks were selected. This occurs typically in forests, which exhibit no discernible threshold. An analysis of individual pixels confirmed this. Spatial Pearson's correlation coefficients of the SM threshold with sand fraction, clay fraction, tree cover and annual precipitation are computed. The soil moisture threshold estimation largely filters out results in forest ecosystems that have increased uncertainties in SM and VWC estimates due to the presence of microwave multiple scattering and attenuation within the canopy[60].

SM threshold values are converted to soil matric potentials using the clay and sand fraction[30] and the Brooks–Corey soil water retention model[61]:

$$\psi(\mathrm{SM}) = \psi_S \left(\frac{\mathrm{SM}}{n}\right)^{-b} \quad (1)$$

ψ, ψ_S, n and b represent soil matric potential, saturated matric potential, porosity and Brooks–Corey parameter, respectively. Standard values of ψ_S, n and b for clay, sand and loam were obtained[62]. Using an approximation that loam fraction is 1 minus the sand and clay fractions, ψ_S, n and b values for each grid cell were obtained through linear weighted averaging of each parameter based on the sand, clay and loam fractions. These values, along with the SM threshold from Supplementary Fig. 3, were used to determine ψ in equation (1).

Estimation of vegetation responsiveness to SM pulses. A pixel-by-pixel analysis is conducted at a 0.5° resolution in which all ΔVWC/ΔSM increments are computed for only SM drydowns greater than the SM threshold estimated in Supplementary Fig. 3. Of these increments, the median ΔVWC/ΔSM is then computed and reported as in Fig. 4. The median was selected as the best metric, as often the distribution included ΔVWC/ΔSM increments of ±infinity when ΔSM approached zero. The same analysis is repeated for SM drydowns lower than the SM threshold and is reported in Supplementary Fig. 5.

Uncertainty estimates with bootstrapping. Bootstrapping is used to develop uncertainty estimates for SM thresholds and median ΔVWC/ΔSM values. This is conducted for each 0.5° pixel. For SM thresholds, all drydowns used to estimate thresholds in Fig. 3 are compiled and sampled with replacement for the same number of trials as the number of drydowns. An SM threshold is generated for each trial in the same way as in the SM and soil matric potential threshold estimation section. This is repeated 2,000 times to generate a SM threshold distribution for each pixel. Similarly, all ΔVWC/ΔSM increments used to compute the median ΔVWC/ΔSM for each pixel are compiled and sampled with replacement for the same number of trials as there are increments for each pixel. The median value is calculated to generate a ΔVWC/ΔSM value. This is repeated 10,000 times to generate a ΔVWC/ΔSM distribution for each pixel. A sample cumulative distribution function with binned boxplots shows the uncertainty bounds for each 10th percentile of the SM threshold and ΔVWC/ΔSM in Supplementary Fig. 7.

Dataset assessment. The SMAP L3 enhanced SM product has been shown to compare closely with in situ SM measurements at calibration/validation sites with an average bias of −0.02 $m^3 m^{-3}$ and root mean square error (RMSE) of 0.061 $m^3 m^{-3}$ (ref. [63]). At these sites, the retrieved MT-DCA SM is highly correlated with the validated SMAP SM enhanced product (average $r = 0.93$; $P < 0.01$). The retrieved MT-DCA τ, however, has a far lower correlation with the SMAP baseline τ product generated from a connectivity model based on empirical

relationships and MODIS normalized difference vegetation index (NDVI) (average $r=0.11$; $P<0.15$). This is no surprise given that MODIS NDVI represents top-of-canopy properties (for example, greenness), while τ represents within-canopy properties (biomass and VWC)[64]. Additionally, the MT-DCA SM has comparison statistics (for example, unbiased root mean square difference, root mean square difference, bias and correlation) with the in situ SM measurements similar to the SMAP SM. See Konings et al.[52,53] for more details on MT-DCA SM comparisons. Unfortunately, there are no known in situ data available to validate τ, especially temporal dynamics. However, MT-DCA τ and independently retrieved τ from the Soil Moisture Ocean Salinity (SMOS) satellite[65] compare closely with spatial correlation of their temporal means ($r=0.93$; $P<0.01$) and temporal correlation of seasonal amplitude (same smoothing procedure as applied in the Characterization of SM drydowns and VWC–SM phase space section; median spatial $r=0.62$; $P<0.01$). The raw temporal correlation is lower (median spatial $r=0.17$; $P<0.05$). See Konings et al.[53] for more information on SMAP and SMOS τ comparisons.

Code availability. The code used to compute and plot metrics in this study can be accessed at https://github.com/afeld24/Plant-Soil-Water-Relations.

Reporting Summary. Further information on research design is available in the Nature Research Reporting Summary linked to this article.

Data availability

SMAP L1C brightness temperature and ancillary datasets are freely available on National Snow and Ice Data Center (NSIDC) (https://nsidc.org/data/SPL1CTB_E/versions/1). IGBP land-cover classifications are freely available through NASA (https://modis.gsfc.nasa.gov/data/dataprod/mod12.php). MODIS tree-cover fraction is freely available through NASA (https://modis.gsfc.nasa.gov/data/dataprod/mod44.php). The GPM Version 5 IMERG precipitation product is freely available through NASA (https://pmm.nasa.gov/data-access/downloads/gpm). Responsiveness and soil moisture threshold metrics are available at https://github.com/afeld24/Plant-Soil-Water-Relations. MT-DCA SM and τ retrievals are available from the corresponding author upon request.

Received: 8 June 2018; Accepted: 15 October 2018;
Published online: 3 December 2018

References

1. Yang, L. H., Bastow, J. L., Spence, K. O. & Wright, A. N. What can we learn from resource pulses? *Ecology* **89**, 621–634 (2008).
2. Reynolds, J. F., Kemp, P. R., Ogle, K. & Fernández, R. J. Modifying the 'pulse-reserve' paradigm for deserts of North America: precipitation pulses, soil water, and plant responses. *Oecologia* **141**, 194–210 (2004).
3. Ogle, K. & Reynolds, J. F. Plant responses to precipitation in desert ecosystems: integrating functional types, pulses, thresholds, and delays. *Oecologia* **141**, 282–294 (2004).
4. BassiriRad, A. H. et al. Short-term patterns in water and nitrogen acquisition by two desert shrubs following a simulated summer rain. *Plant Ecol.* **145**, 27–36 (1999).
5. Montaña, C., Cavagnaro, B. & Briones, O. Soil water use by co-existing shrubs and grasses in the southern Chihuahuan Desert, Mexico. *J. Arid Environ.* **31**, 1–13 (1995).
6. Sala, O. E., Lauenroth, W. K. & Parton, W. J. Plant recovery following prolonged drought in a shortgrass steppe. *Agric. Meteorol.* **27**, 49–58 (1982).
7. Sala., O. E. & Lauenroth, W. K. Small rainfall events: an ecological role in semiarid regions. *Oecologia* **53**, 301–304 (1982).
8. Noy-Meir, I. Desert ecosystems: environment and producers. *Annu. Rev. Ecol. Syst.* **4**, 25–52 (1973).
9. Schwinning, S., Sala, O. E., Loik, M. E. & Ehleringer, J. R. Thresholds, memory, and seasonality: understanding pulse dynamics in arid/semi-arid ecosystems. *Oecologia* **141**, 191–193 (2004).
10. Chen, S., Lin, G., Huang, J. & Jenerette, D. Dependence of carbon sequestration on the differential responses of ecosystem photosynthesis and respiration to rain pulses in a semiarid steppe. *Glob. Change Biol.* **15**, 2450–2461 (2009).
11. Huxman, T. E. et al. Precipitation pulses and carbon fluxes in semiarid and arid ecosystems. *Oecologia* **141**, 254–268 (2004).
12. Schwinning, S. & Sala, O. E. Hierarchy of responses to resource pulses in arid and semi-arid ecosystems. *Oecologia* **141**, 211–220 (2004).
13. Fisher, R. A. et al. Vegetation demographics in Earth system models: a review of progress and priorities. *Glob. Change Biol.* **24**, 35–54 (2018).
14. Asbjornsen, H. et al. Ecohydrological advances and applications in plant–water relations research: a review. *J. Plant Ecol.* **4**, 3–22 (2011).
15. Jasechko, S. et al. Terrestrial water fluxes dominated by transpiration. *Nature* **496**, 347–350 (2013).
16. Entekhabi, D. et al. The soil moisture active passive (SMAP) mission. *Proc. IEEE* **98**, 704–716 (2010).
17. Jones, M. O., Jones, L. A., Kimball, J. S. & McDonald, K. C. Satellite passive microwave remote sensing for monitoring global land surface phenology. *Remote Sens. Environ.* **115**, 1102–1114 (2011).
18. Tian, F. et al. Coupling of ecosystem-scale plant water storage and leaf phenology observed by satellite. *Nat. Ecol. Evol.* **2**, 1428–1435 (2018).
19. Konings, A. G. & Gentine, P. Global variations in ecosystem-scale isohydricity. *Glob. Change Biol.* **23**, 891–905 (2017).
20. Momen, M. et al. Interacting effects of leaf water potential and biomass on vegetation optical depth. *J. Geophys. Res. Biogeosci.* **122**, 3031–3046 (2017).
21. Brandt, M. et al. Satellite passive microwaves reveal recent climate-induced carbon losses in African drylands. *Nat. Ecol. Evol.* **2**, 827–835 (2018).
22. Donat, M. G., Lowry, A. L., Alexander, L. V., O'Gorman, P. A. & Maher, N. More extreme precipitation in the world's dry and wet regions. *Nat. Clim. Change* **6**, 508–513 (2016).
23. Feng, X., Porporato, A. & Rodriguez-Iturbe, I. Changes in rainfall seasonality in the tropics. *Nat. Clim. Change* **3**, 811–815 (2013).
24. Fisher, J. B. et al. African tropical rainforest net carbon dioxide fluxes in the twentieth century. *Philos. T. R. Soc. B* **368**, 20120376–20120376 (2013).
25. Zhou, L. et al. Widespread decline of Congo rainforest greenness in the past decade. *Nature* **508**, 86–90 (2014).
26. Beer, C. et al. Terrestrial gross carbon dioxide uptake: global distribution and covariation with climate. *Science* **329**, 834–838 (2010).
27. Poulter, B. et al. Contribution of semi-arid ecosystems to interannual variability of the global carbon cycle. *Nature* **509**, 600–603 (2014).
28. Xu, X., Medvigy, D., Powers, J. S., Becknell, J. M. & Guan, K. Diversity in plant hydraulic traits explains seasonal and inter-annual variations of vegetation dynamics in seasonally dry tropical forests. *New Phytol.* **212**, 80–95 (2016).
29. McColl, K. A. et al. Global characterization of surface soil moisture drydowns. *Geophys. Res. Lett.* **44**, 3682–3690 (2017).
30. Golluscio, A. R. A., Sala, O. E. & Lauenroth, W. K. Differential use of large summer rainfall events by shrubs and grasses: a manipulative experiment in the Patagonian steppe. *Oecologia* **115**, 17–25 (1998).
31. Meinzer, F. C. et al. Converging pattern of hydraulic redistribution of soil water in contrasting woody vegetation types. *Tree Physiol.* **24**, 919–928 (2004).
32. Zhang, Q., Manzoni, S., Katul, G., Porporato, A. & Yang, D. The hysteretic evapotranspiration–vapor pressure deficit relation. *J. Geophys. Res. Biogeosci.* **119**, 125–140 (2014).
33. Feddes, R. A. et al. Modeling root water uptake in hydrological and climate models. *Bull. Am. Meteorol. Soc.* **82**, 2797–2809 (2001).
34. Becker, P. & Castillo, A. Root architecture of shrubs and saplings in the understory of a tropical moist forest in lowland Panama. *Biotropica* **22**, 242–249 (1990).
35. Le Roux, X., Bariac, T. & Mariotti, A. Spatial partitioning of the soil water resource between grass and shrub components in a West African humid savanna. *Oecologia* **104**, 147–155 (1995).
36. Meinzer, F. C. et al. Partitioning of soil water among canopy trees in a seasonally dry tropical forest. *Oecologia* **121**, 293–301 (1999).
37. Jackson, R. B. et al. A global analysis of root distributions for terrestrial biomes. *Oecologia* **108**, 389–411 (1996).
38. Schenk, J. H. & Jackson, R. B. The global biogeography of roots. *Ecol. Monogr.* **72**, 311–328 (2002).
39. Dara, A., Moradi, B. A., Vontobel, P. & Oswald, S. E. Mapping compensating root water uptake in heterogeneous soil conditions via neutron radiography. *Plant Soil* **397**, 273–287 (2015).
40. Laio, F., Porporato, A., Fernandez-Illescas, C. P. & Rodriguez-Iturbe, I. Plants in water-controlled ecosystems: active role in hydrologic processes and response to water stress IV. Discussion of real cases. *Adv. Water Resour.* **24**, 745–762 (2001).
41. Emanuel, R. E., D'Odorico, P. & Epstein, H. E. A dynamic soil water threshold for vegetation water stress derived from stomatal conductance models. *Water Resour. Res.* **43**, 1–13 (2007).
42. Rodriguez-Iturbe, I., D'Odorico, P., Laio, F., Ridolfi, L. & Tamea, S. Challenges in humid land ecohydrology: interactions of water table and unsaturated zone with climate, soil, and vegetation. *Water Resour. Res.* **43**, 1–5 (2007).
43. Lin, Y. S. et al. Optimal stomatal behaviour around the world. *Nat. Clim. Change* **5**, 459–464 (2015).
44. Fan, Y., Miguez-Macho, G., Jobbágy, E. G., Jackson, R. B. & Otero-Casal, C. Hydrologic regulation of plant rooting depth. *Proc. Natl Acad. Sci. USA* **114**, 10572–10577 (2017).
45. Tai, X., Mackay, D. S., Anderegg, W. R. L., Sperry, J. S. & Brooks, P. D. Plant hydraulics improves and topography mediates prediction of aspen mortality in southwestern USA. *New Phytol.* **213**, 113–127 (2017).
46. Chaubell, J., Chan, S., Dunbar, R. S., Peng, J. & Yueh., S. *SMAP Enhanced L1C Radiometer Half-Orbit 9 km EASE-Grid Brightness Temperatures, Version 1* (NASA National Snow and Ice Data Center Distributed Active Archive Center, 2016); https://doi.org/10.5067/2C9O9KT6JAWS

47. Chaubell, J., Yueh, S., Entekhabi, D. & Peng, J. Resolution enhancement of SMAP radiometer data using the Backus Gilbert optimum interpolation technique in *2016 IEEE International Geoscience and Remote Sensing Symposium* 284–287 (IEEE, 2016).
48. Huffman, G. *GPM Level 3 IMERG Final Run Half Hourly 0.1 × 0.1 Degree Precipitation, Version 05* (Goddard Space Flight Center Distributed Active Archive Center, 2015).
49. Dimiceli, C. et al. *MOD44B MODIS/Terra Vegetation Continuous Fields Yearly L3 Global 250m SIN Grid V006* (NASA EOSDIS Land Processes DAAC, 2015); https://doi.org/10.5067/MODIS/MOD44B.006
50. Kim, S. *Ancillary Data Report: Landcover Classification* D-53057 (Jet Propulsion Laboratory California Institute of Technology, 2013).
51. Mo, T., Choudhury, B. J., Schmugge, T. J., Wang, J. R. & Jackson, T. J. A model for microwave emission from vegetation-covered fields. *J. Geophys. Res.* **87**, 11229 (1982).
52. Konings, A. G. et al. Vegetation optical depth and scattering albedo retrieval using time series of dual-polarized L-band radiometer observations. *Remote Sens. Environ.* **172**, 178–189 (2016).
53. Konings, A. G., Piles, M., Das, N. & Entekhabi, D. L-band vegetation optical depth and effective scattering albedo estimation from SMAP. *Remote Sens. Environ.* **198**, 460–470 (2017).
54. Jackson, T. J. & Schmugge, T. J. Vegetation effects on the microwave emission of soils. *Remote Sens. Environ.* **36**, 203–212 (1991).
55. O'Neill, P. *Soil Moisture Active Passive (SMAP) Algorithm Theoretical Basis Document (ATBD) SMAP Level 2 & 3 Soil Moisture (Passive)* (Jet Propulsion Laboratory California Institute of Technology, 2012).
56. Wigneron, J. P. et al. Modelling the passive microwave signature from land surfaces: a review of recent results and application to the L-band SMOS & SMAP soil moisture retrieval algorithms. *Remote Sens. Environ.* **192**, 238–262 (2017).
57. O'Neill, P. E., Chan, S., Njoku, E. G., Jackson, T. & Bindlish, R. *SMAP Enhanced L3 Radiometer Global Daily 9 km EASE-Grid Soil Moisture, Version 1* (NASA National Snow and Ice Data Center Distributed Active Archive Center, 2016); https://doi.org/10.5067/ZRO7EXJ8O3XI
58. Dezfuli, A. K. et al. Validation of IMERG precipitation in Africa. *J. Hydrometeorol.* **18**, 2817–2825 (2017).
59. Tuttle, S. E. & Salvucci, G. D. Confounding factors in determining causal soil moisture-precipitation feedback. *Water Resour. Res.* **53**, 5531–5544 (2017).
60. Kurum, M. et al. A first-order radiative transfer model for microwave radiometry of forest canopies at L-band. *IEEE. Trans. Geosci. Remote. Sens.* **49**, 3167–3179 (2011).
61. Brooks, R. H. & Corey, A. T. Properties of porous media affecting fluid flow. *J. Irrig. Drain. Div.* **92**, 61–90 (1966).
62. Clapp, R. B. & Hornberger, G. M. Empirical equations for some soil hydraulic properties. *Water Resour. Res.* **14**, 601–604 (1978).
63. Chan, S. K. et al. Assessment of the SMAP passive soil moisture product. *IEEE. Trans. Geosci. Remote Sens.* **54**, 4994–5007 (2016).
64. Liu, Y. Y., De Jeu, R. A. M., McCabe, M. F., Evans, J. P. & Van Dijk, A. I. J. M. Global long-term passive microwave satellite-based retrievals of vegetation optical depth. *Geophys. Res. Lett.* **38**, 1–6 (2011).
65. Kerr, Y. et al. The SMOS mission: new tool for monitoring key elements of the global water cycle. *Proc. IEEE* **98**, 666–687 (2010).

Acknowledgements

Massachusetts Institute of Technology contributors were supported under contract with NASA. K.A.M. was funded by a Ziff Environmental Fellowship from Harvard University's Center for the Environment. A.G.K. was supported by NASA Terrestrial Ecology award no. 80NSSC18K0715 through the New Investigator programme.

Author contributions

A.F.F. and D.E. conducted the analysis. A.F.F. wrote the manuscript. D.E. conceived and led the project. D.J.S.G., A.G.K., K.A.M., R.A. and G.D.S. contributed to interpretations of results as well as revisions to various versions of the analyses, figures and manuscripts.

Competing interests

The authors declare no competing interests.

Additional information

Supplementary information is available for this paper at https://doi.org/10.1038/s41477-018-0304-9.

Reprints and permissions information is available at www.nature.com/reprints.

Correspondence and requests for materials should be addressed to A.F.F.

Publisher's note: Springer Nature remains neutral with regard to jurisdictional claims in published maps and institutional affiliations.

nature research

Corresponding author(s): Andrew F. Feldman

Reporting Summary

Nature Research wishes to improve the reproducibility of the work that we publish. This form provides structure for consistency and transparency in reporting. For further information on Nature Research policies, see Authors & Referees and the Editorial Policy Checklist.

Statistical parameters

When statistical analyses are reported, confirm that the following items are present in the relevant location (e.g. figure legend, table legend, main text, or Methods section).

n/a	Confirmed	
☐	☒	The exact sample size (*n*) for each experimental group/condition, given as a discrete number and unit of measurement
☐	☒	An indication of whether measurements were taken from distinct samples or whether the same sample was measured repeatedly
☐	☒	The statistical test(s) used AND whether they are one- or two-sided *Only common tests should be described solely by name; describe more complex techniques in the Methods section.*
☒	☐	A description of all covariates tested
☒	☐	A description of any assumptions or corrections, such as tests of normality and adjustment for multiple comparisons
☒	☐	A full description of the statistics including central tendency (e.g. means) or other basic estimates (e.g. regression coefficient) AND variation (e.g. standard deviation) or associated estimates of uncertainty (e.g. confidence intervals)
☒	☐	For null hypothesis testing, the test statistic (e.g. *F*, *t*, *r*) with confidence intervals, effect sizes, degrees of freedom and *P* value noted *Give P values as exact values whenever suitable.*
☒	☐	For Bayesian analysis, information on the choice of priors and Markov chain Monte Carlo settings
☒	☐	For hierarchical and complex designs, identification of the appropriate level for tests and full reporting of outcomes
☒	☐	Estimates of effect sizes (e.g. Cohen's *d*, Pearson's *r*), indicating how they were calculated
☒	☐	Clearly defined error bars *State explicitly what error bars represent (e.g. SD, SE, CI)*

Our web collection on statistics for biologists may be useful.

Software and code

Policy information about availability of computer code

Data collection	SMAP L1C_E (9 kilometer) brightness temperature data were downloaded from NASA (search.earthdata.nasa.gov) using a Bash command (using Bash on Ubuntu on Windows). MATLAB R2016b and a written script were used to estimate soil moisture and vegetation water content data on a cluster in the MIT Mathematics Department. Processed soil moisture and vegetation water content .mat files as well as retrieval script .m file are available from authors on request.
Data analysis	MATLAB R2016b was used to analyze data. .m files used to analyze data are available from authors upon request.

For manuscripts utilizing custom algorithms or software that are central to the research but not yet described in published literature, software must be made available to editors/reviewers upon request. We strongly encourage code deposition in a community repository (e.g. GitHub). See the Nature Research guidelines for submitting code & software for further information.

Data

Policy information about availability of data

All manuscripts must include a data availability statement. This statement should provide the following information, where applicable:

- Accession codes, unique identifiers, or web links for publicly available datasets
- A list of figures that have associated raw data
- A description of any restrictions on data availability

Raw SMAP brightness temperature data are available at https://nsidc.org/data/SPL1CTB_E/versions/2. Note that this data is Version 2 while we use Version 1 when we downloaded in August 2017. We have archived the Version 1 dataset and it is available for use upon request. Please note that converting this to soil moisture and vegetation water content requires time and computation power. The methods for doing so are outlined in Konings et al. (2016), an article referenced in our manuscript. While we have not made our vegetation water content and soil moisture datasets publicly available due to file size, we can provide these for use by the editors and reviewers. They are three dimensional gridded data in .mat files compiled into 6 months ranging between 300 and 1 GB each for a total of about 10 GB. Also, all code as well as soil moisture threshold and vegetation responsiveness estimates are available at https://github.com/afeld24/Plant-Soil-Water-Relations.

Land cover classifications are freely available through NASA (https://modis.gsfc.nasa.gov/data/dataprod/mod12.php). MODIS tree cover fraction are also freely available through NASA (https://modis.gsfc.nasa.gov/data/dataprod/mod44.php).

Field-specific reporting

Please select the best fit for your research. If you are not sure, read the appropriate sections before making your selection.

☐ Life sciences ☐ Behavioural & social sciences ☒ Ecological, evolutionary & environmental sciences

For a reference copy of the document with all sections, see nature.com/authors/policies/ReportingSummary-flat.pdf

Ecological, evolutionary & environmental sciences study design

All studies must disclose on these points even when the disclosure is negative.

Study description	This study was conducted using remote sensing data of passive low frequency microwave emission from the land surface over Africa, Australia, and South America. This emission is highly sensitive to the water content of the uppermost soil layer and of the overlying vegetation. We analyze the short term variations (~2-3 days apart) of these water contents during "soil moisture drydowns" which are periods following a rain event when the surface is overall drying over a multi-day period.
Research sample	The sample is all 9 km SMAP grid cells over Africa, Australia, and South America. These continents contain a vast expanse of contrasting biomes with many pixels with a low water body fraction. Increased standing water body area can significantly contaminate the SMAP radiometer measurements and introduce errors in estimating soil moisture and vegetation water content.
Sampling strategy	After the regions of pixels were selected, sampling was conducted over time. In this study, only soil moisture and vegetation water content estimates during soil moisture drydowns were sampled from the study. Soil moisture drydowns are consecutive drying periods where soil moisture is consecutively less than the previous time of measurement. Only soil moisture drydowns with greater than or equal to four consecutive measurements (with soil moisture less than the previous day) were sampled in each 9 km pixel. The choice of four consecutive overpasses is a balance between removing short unphysical SM drydowns due to SMAP satellite radiometer noise and avoiding a bias of only evaluating the longest drydowns.
Data collection	The data collection is completed by the SMAP satellite's radiometer. Pre-processing of data such as any calibration and error correction is completed by NASA's SMAP science team. The authors' data collection procedure consisted of downloading the data from NASA's data website which is described in the "Data" section of this document. Data collection of soil moisture and vegetation water content during soil moisture drydowns was completed using Bash (see Software and Code section) by the authors.
Timing and spatial scale	This study was conducted in all 9 km SMAP grid cells over Africa, Australia, and South America from April 1st, 2015 to December 26th, 2017 which when downloaded and processed (after December 27th, 2017) was the longest extent of SMAP measurements.
Data exclusions	Brightness temperature measurements excluded from the analysis were those under frozen temperatures as assumptions in converting to soil moisture and vegetation water content break down. Additionally, all values within pixels that contained greater than 5% water body fraction were removed due to significant water body contamination of SMAP brightness temperature measurements.
Reproducibility	All attempts to repeat the experiment were successful.
Randomization	The study was largely deterministic. Estimated soil moisture thresholds and responsiveness to soil moisture pulses values were binned based on land cover classification or into tree cover percentage groups in Figs. 3 and 4.
Blinding	Given the nature of the data collection where no living subjects were a part of the data collection and processing, blinding is not possible for this study.

Did the study involve field work? ☐ Yes ☒ No

Reporting for specific materials, systems and methods

Materials & experimental systems

n/a	Involved in the study
☒	☐ Unique biological materials
☒	☐ Antibodies
☒	☐ Eukaryotic cell lines
☒	☐ Palaeontology
☒	☐ Animals and other organisms
☒	☐ Human research participants

Methods

n/a	Involved in the study
☒	☐ ChIP-seq
☒	☐ Flow cytometry
☒	☐ MRI-based neuroimaging